Deutsche Hydrographische Zeitschrift
German Journal of Hydrography
Volume 48 (1996) Number 2

ISSN 0012-0308

Near-Bottom Currents and Bottom Boundary Layer Variability Over Manganese Nodule Fields in the Peru Basin, SE-Pacific

HOLGER KLEIN

Summary

Near-bottom current meter data recorded between 0.6 and 500 metres above bottom (mab) at two manganese nodule sites in the deep Peru Basin are discussed with respect to the vertical current structure and the formation and variability of the benthic boundary layer (BBL) and its sublayers. The data reveal a weak current regime with great spatial and temporal variability and a bottom intensification at about 30–50 mab. The BBL height varies according to the daily mean values of flow above the BBL, reaching maximally 150 to 200 metres.

Bodennahe Strömungen und Bodengrenzschichtvariabilität über Manganknollenfeldern im Peru Becken, SO-Pazifik (Zusammenfassung)

Bodennahe Strommessungen (0,6 bis 500 m Bodenabstand) aus zwei Manganknollengebieten im Peru Becken werden bezüglich des vertikalen Stromprofils und der Bildung und Variabilität der Bodengrenzschicht und ihrer Unterschichten diskutiert. Die Daten zeigen ein schwaches Strömungsregime mit großer zeitlicher und räumlicher Variabilität und einer Bodenintensivierung der Strömung bei etwa 30 bis 50 m Bodenabstand. Die Höhe der Bodengrenzschicht variiert entsprechend den täglichen Mittelwerten der Strömung über der Bodengrenzschicht und erreicht eine maximale Höhe von 150 bis 200 m.

Introduction

Since 1988, the TUSCH-group[1], a multidisciplinary association of research groups, has investigated the potential impact of deep-sea manganese nodule mining on the abyssal ecosystem of the Peru Basin (THIEL AND SCHRIEVER [1989], THIEL et al. [1994], THIEL [1995]). During the DISCOL[2] experiment in 1989, part of the DISCOL Experimental Area (DEA) was disturbed using a towed plow-harrow in order to simulate a mining operation and to investigate the subsequent recolonization of local benthic communities (SCHRIEVER [1995]). Biological, geological, geochemical, and soil-mechanical investigations in the DEA and surrounding undisturbed areas were carried out before the disturbance, directly after the disturbance, and in subsequent years (SCHRIEVER et al. [1996]).

Besides the direct disturbance of the sea bed, the influence of settling sediments – mobilized during mining operations – has to be considered. Mobilized sediment plumes are dispersed according to local current strength and current variability. Resedimentation of advected suspended particles may also affect areas beyond the mining sites proper. Moreover, the local current regime – together with bottom roughness and topography – controls the properties of the bottom or benthic boundary layer (BBL) and its variability. Knowledge about the BBL structure is of great significance because local chemistry, biology, and physics of the BBL are closely interwined (BERNER [1976]).

[1] TUSCH = Tiefsee-Umweltschutz = deep-sea environmental protection
[2] DISCOL = Disturbance and recolonization experiment in the South Pacific

The Peru Basin is formed by the Carnegie Ridge and the Galapagos Spreading Centre to the north, the Nazca and Sala-y-Gomez Ridge to the south, and the East Pacific Rise at its western margin (see Fig. 1). The deep water in this basin is of southern origin. It branches off from the circumpolar current and flows through a pair of unnamed transform faults of the Chile Rise into the Chile Basin. From there, it enters the Peru Basin via the Peru-Chile Trench and a sill between the Nazca and Sala-y-Gomez Ridge (LONSDALE [1976]). According to WARREN [1981], the abyssal flow in the Peru Basin is very diffuse and does not look 'current-like'. Bottom photograph interpretation shows no evidence of current activity in the Peru Basin; only some cases of epifauna deflection could be detected. Like other large areas of the North and South Pacific, the basin is relatively free of sediment-transporting current activity (HOLLISTER AND NOWELL [1991]). Within the framework of TUSCH, the BSH[3] deployed three current meter moorings in the basin in order to quantify near-bottom current intensity and to estimate possible transport rates of suspended material.

Table 1

Deployment data

mab	depth	sampling rate	number of cycles	days	rotor[1] stalls	sampling time
m	m	min	–	–	%	–
D1: 7° 4.1' S, 88° 28.2' W, water depth 4143 m						
200	3943	180	6886	861	19.1	23.09.89–31.01.92
50	4093	180	6886	861	20.6	23.09.89–31.01.92
30	4113	60	9612	400	26.3	23.09.89–28.10.90
15	4128	180	6886	861	11.5	23.09.89–31.01.92
MK1: 6° 31.5' S, 90° 24.8' W, water depth 4139 m						
503	3636	10	6878	48	64.3	08.01.96–25.02.96
202	3937	10	6463	45	62.7	08.01.96–22.02.96
50	4089	10	7142	50	53.1	08.01.96–27.02.96
13	4126	5	14990	52	86.0	08.01.96–29.02.96
4	4135	5	14999	52	88.8	08.01.96–29.02.96
0.6	4138	5	14981	52	87.5	08.01.96–29.02.96
MK2: 7° 4.3' S, 88° 32.0' W, water depth 4149 m						
503	3646	10	6894	48	46.7	10.01.96–27.02.96
202	3947	10	7610	53	60.7	10.01.96–03.03.96
50	4099	10	6674	46	48.8	10.01.96–26.01.96
13	4136	5	15217	53	73.2	10.01.96–03.03.96
4	4145	5	15238	53	76.2	10.01.96–03.03.96

mab = metres above bottom

[1] The threshold velocity of the current meters is 1–1.5 cm/s

[3] BSH = Bundesamt für Seeschiffahrt und Hydrographie (Federal Maritime and Hydrographic Agency)

First data came from long-term mooring D1 deployed in DEA for about 28 months (861 days), from September 1989 to January 1992 (R/V 'SONNE' cruises 64 and 77). Samples were taken by Aanderaa RCM5 current meters at 15, 30, 50, and 200 metres above bottom (mab). The sampling rate was 180 minutes at 200, 50, and 15 mab, and 60 minutes at 30 mab. Data recording at 30 mab stopped after 400 days due to limited capacity of the magnetic tape (see Table 1). The results of this deployment are discussed in detail by KLEIN [1993].

Four years later, two short-term moorings were deployed from January 1996 until March 1996 during R/V 'Sonne' cruise 106 within the framework of ATESEPP[4]: the MK1 mooring in the SEDIPERU area, and the MK2 mooring in DEA (see Fig. 1). These deployments were maintained for only about 52 days, but the sampling intervals were much shorter and the bottom instruments were closer to the seabed. The identically designed moorings were equipped with Aanderaa RCM8 current meters at 0.6, 4, 13, 50, 202, and 503 mab (KLEIN [1996]). The sampling rate was 5 minutes at 0.6, 4, and 13 mab, and 10 minutes for the upper instruments. At MK2, no data were obtained from 0.6 mab due to failure of the data storing unit. Unfortunately, both moorings did not provide information on the current direction at 0.6 and 4 mab. The cause of the failure was not found.

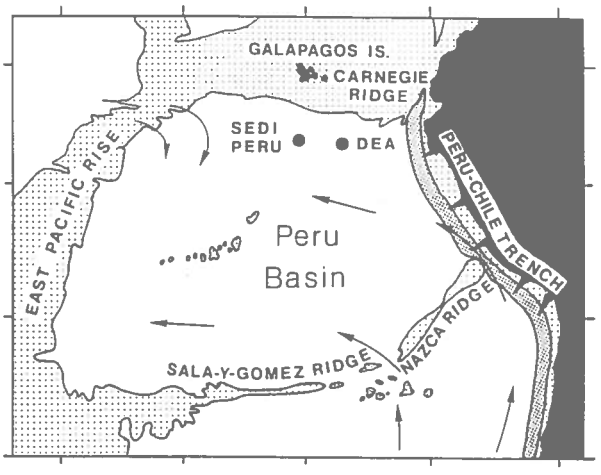

Fig.1: Location of the DISCOL Experimental Area (DEA) with moorings D1 and MK2 and of the SEDIPERU site with mooring MK1. Light spotted areas are shallower than 3500 metres. The arrows schematically outline the circulation of bottom water according to LONSDALE [1976].

Topography and bottom roughness

The DEA proper is a cirular site centered at 7° 4.4' S, 88° 27.6' W with a diameter of 2 nautical miles (nm) and an area of 10.8 km² (spotted circle in Fig. 2), located at the northeastern margin of the Peru Basin nodule field. The depth varies between 4140 and 4170 m. D1 lies in the western part of DEA, MK2 about 5 nm west of the DEA centre. 2 nm north of DEA lies a hill of 300 m height and a maximum slope of 10°. Depths around the disturbed area vary between 3890 and 4220 m.

Investigations at the SEDIPERU site focus on the area around a 250 m high conical volcanic hill at 6° 32' S, 90° 28' W which is surrounded by a relatively flat area with a fairly thick sediment cover (see Fig. 2). Depths vary between 3900 and 4300 m. MK1 lies 2 nm east of the foot of the hill.

The Peru Basin is characterized by the occurrence of extremely large nodules with maximum diameters of up to 21 cm, while nodules smaller than 1.5 cm are scarce (VON STACKELBERG [1997]). The largest number of nodules per m² is found on top of the seamounts. At both sites, areas with dense nodule coverage are adjacent to erosional areas which are basically free of manganese nodules. Photo-sledge profiles show a very rapid transition between these areas (WIEDECKE AND WEBER [1996]). The diameter of the nodules generally varies between 2 and 13 cm, the majority measuring 3 to 5 cm (see Fig. 3). The number of nodules found on the surface of box corer samples during Sonne cruise 106 ranges between 1 and 143 nodules at the DEA, and between 1 and 86 nodules at the SEDIPERU site (SCHRIEVER et al. [1996]).

[4] ATESEPP = Auswirkungen technischer Eingriffe in das Ökosystem der Tiefsee im Süd-Ost-Pazifik vor Peru = Impacts of potential technical interventions on the deep-sea ecosystem of the southeast Pacific off Peru

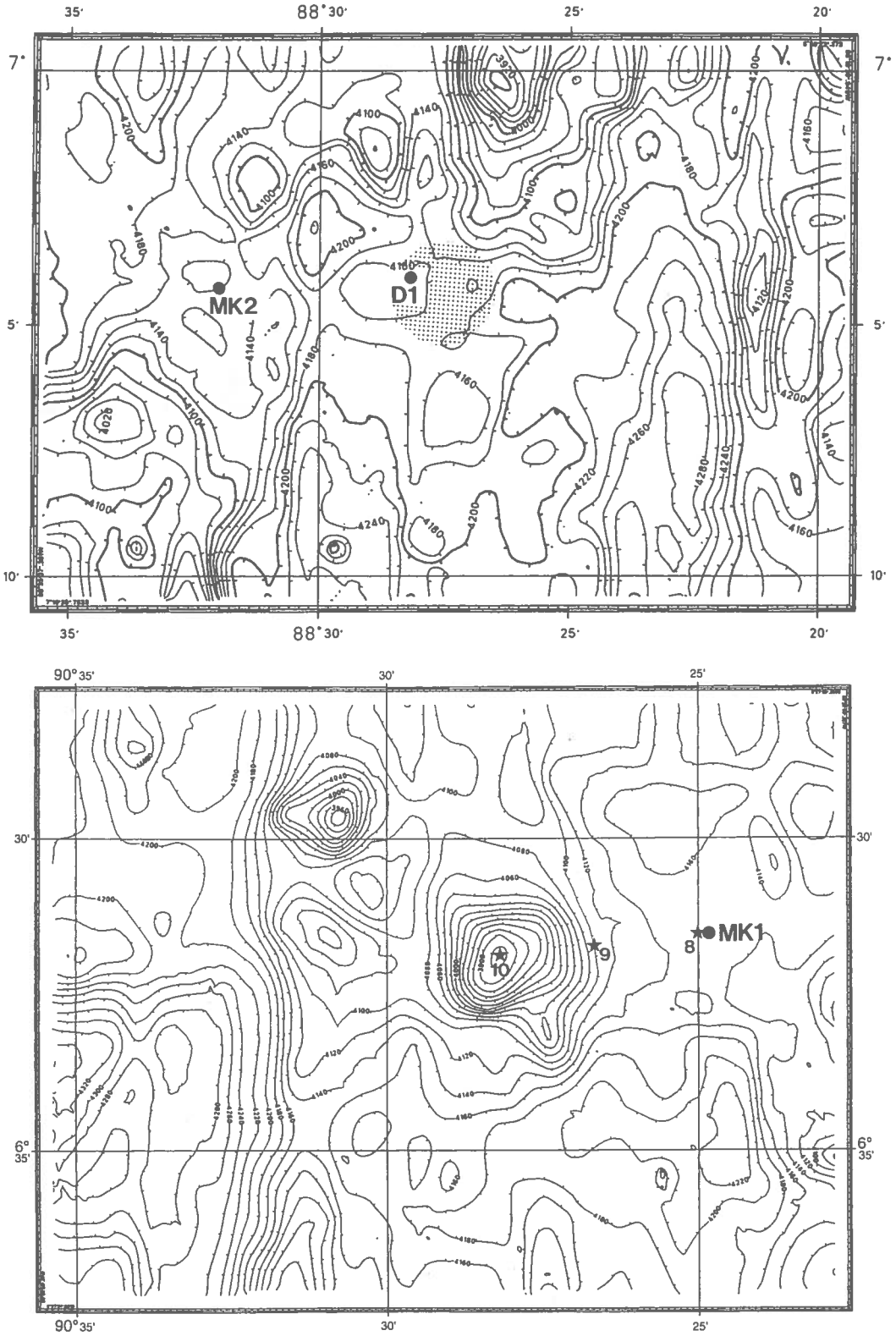

Fig.2: Topography of the DEA (top) and SEDIPERU sites (bottom). The disturbed part of the DEA site is spotted. The mooring positions are marked by dots, the stars mark the positions of CTD stations 8, 9, and 10.

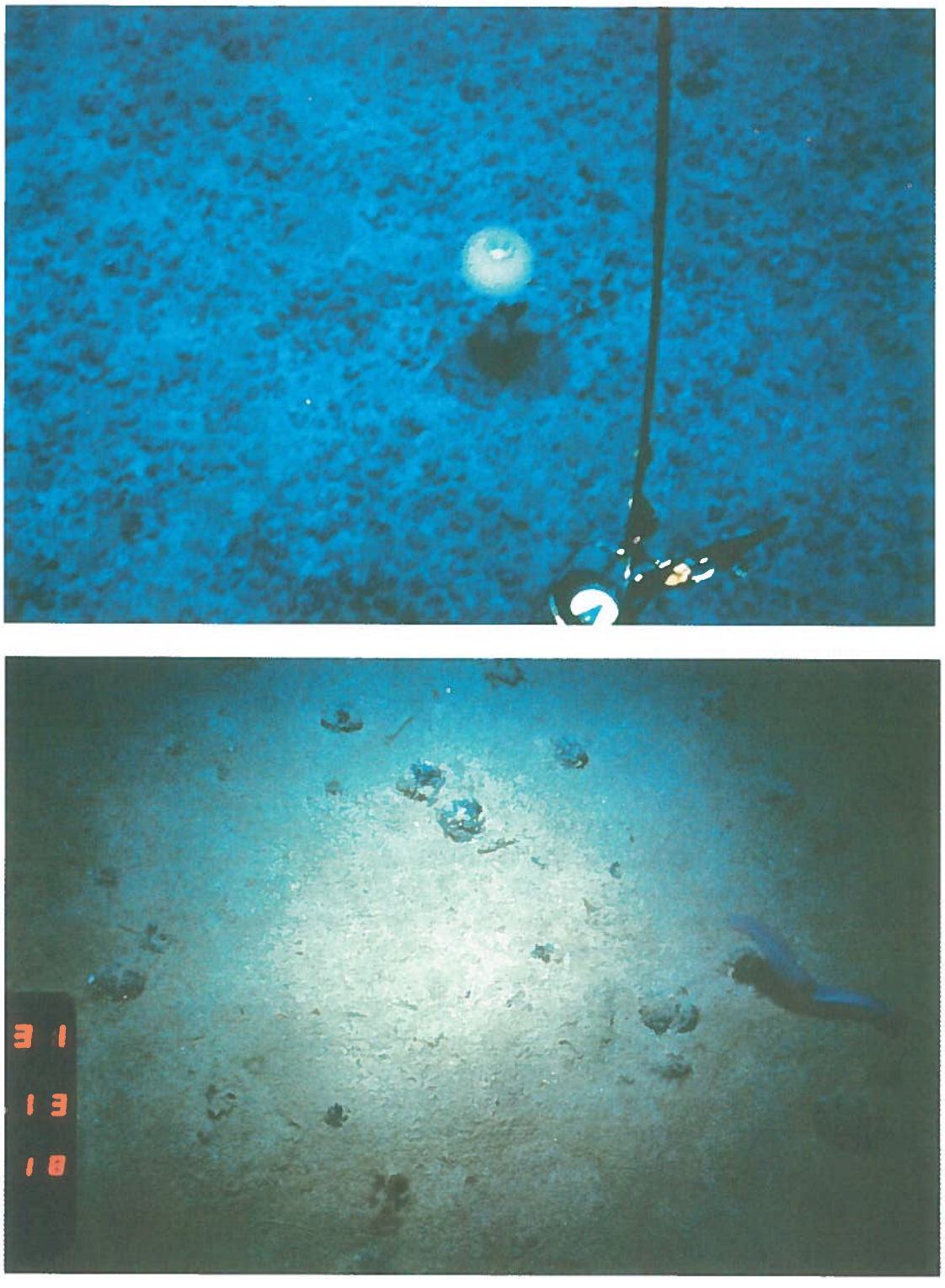

Fig.3: Top: Photograph of the sea bottom with dense manganese nodule coverage. Most of the nodules have diameters between 3 and 5 cm. Bottom: Bottom sediment with fewer but larger nodules. Here the nodule diameters are up to 13 cm. Both types of sea bottom are found at the DEA and SEDIPERU sites. The photographs were kindly provided by H. BLUHM.

This corresponds to a maximum coverage of 572 and 344 nodules per m². Von STACKELBERG [1997] reports a maximum coverage of 910 nodules per m² close to the SEDIPERU site.

Particle diameters in the upper 1 cm of the sediment vary between <20 and about 200 µm at both sites (nodule covered areas). The upper 8 to 10 cm of very soft sediment are called 'semi-liquid layer'. The bottom boundary of the Peru Basin is a low-energetic boundary layer, i. e. there is no erosion due to natural bottom currents (JANKOWSKI AND ZIELKE [1995]). This is confirmed by geological and soil-mechanical investigations at both sites which gave no hints of erosional events.

Near-bottom currents

a) Long-term mooring D1

At the DEA site, the mean velocity magnitude ranges between 2 and 4 cm/s with a clear increase towards the bottom. Rotor stalls were about 10% at 15 mab, and about 20% between 30 and 200 mab (see Table 1). Average stall duration is 1 to 2 cycles (3 to 6 hours). The maximum stall interval was 21 cycles (63 hours) at 200 mab. Between 15 and 50 mab the flow direction is northwest, at 200 mab the mean current runs westward.

The progressive vector diagram (PVD) in Figure 4 shows that the deep flow is characterized by 2 to 5-month periods of relatively strong currents (>5 cm/s) with only few changes in the direction of flow. During these events, the speed significantly exceeds the total mean of 3 to 4 cm/s. For short periods of a few hours, current speed exceeded 10 cm/s and even reached values up to 17 cm/s. Such phases of strong flow alternate with slow current phases (<1–3 cm/s) of comparable duration but a great directional variability. A periodicity or seasonal signal, however, is not discernible.

Basic flow statistics, calculated from unfiltered data, are summarized in Table 2. For rotor stalls the speed was asumed to equal zero. The small stability factor *SF*[5] emphasizes the great variability of the local deep flow. This also holds true if diurnal and semi-diurnal tides are removed by means of a Gaussian low-pass filter. Bottom intensification of the mean kinetic energy k_M[6] and (turbulent) eddy kinetic energy k_E, as frequently seen in the deep-sea, occurred in the bottom 30 metres. Here, turbulent kinetic energy is produced by vertical shear of the mean flow (zero velocity at the bottom!). k_E generally exceeds k_M.

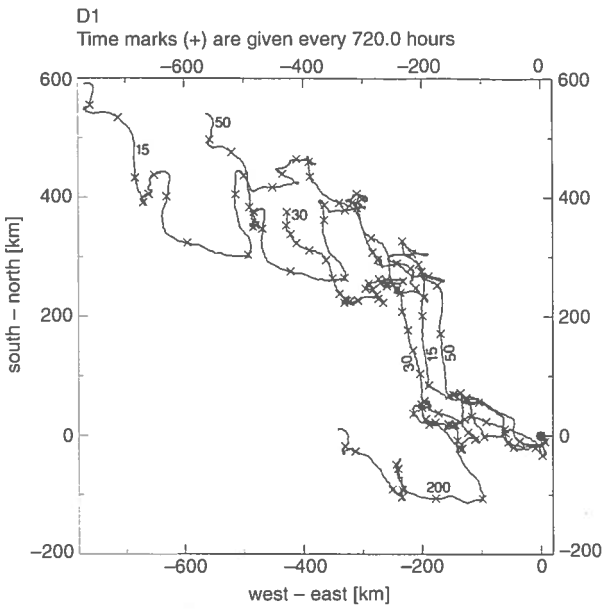

Fig. 4: Progressive vector diagram of long-term mooring D1. Time marks (x) are given every 30 days, the numbers at the tracks give the distance from bottom in metres.

The energy density spectra of the zonal and meridional velocity components show three typical periods of current variability (KLEIN [1993]): The inertial period (4.1 days), the diurnal tide (24.4 h), and the semi-diurnal tide (12 h). However, the tidal currents are very weak, i. e. they are smaller than the threshold velocity of the current meters, thus contributing to the high percentage of rotor stalls (see Table 2).

[5] *SF* = (vector mean/magnitude) x 100. *SF*=100 stands for a constant current direction.
[6] $k_M = 0.5\ (\overline{u}^2+\overline{v}^2)$, $k_E = 0.5\ (\overline{u'u'}+\overline{v'v'})$

Table 2

Current statistics

mab	u	$\overline{u'u'}$	v	$\overline{v'v'}$	$\overline{u'v'}$	V	*mag*	max (*mag*)	*SF*	dir	k_E	k_M	k_E/k_M
m	cm/s	cm²/s²	cm/s	cm²/s²		cm/s	cm/s	cm/s	%	°	cm²/s²		–
D1:													
200	–0.5	4.9	0.0	5.8	–0.6	0.5	2.7	17.1	18	272	5.4	0.1	49
50	–0.8	5.6	0.7	7.2	–0.3	1.0	3.1	11.9	32	314	6.4	0.5	12
30	–1.2	8.4	1.1	8.4	0.5	1.6	3.4	16.8	47	311	7.4	1.3	5
15	–1.0	6.5	0.8	8.6	<–0.1	1.3	3.4	14.7	38	307	7.5	0.9	8
MK1:													
503	–0.1	3.2	–1.1	4.8	1.5	1.1	1.7	8.7	62	186	4.0	0.6	7
202	0.1	2.7	–1.0	5.2	1.0	1.0	1.8	7.8	56	172	3.9	0.5	8
50	0.4	2.4	–0.7	7.1	0.5	0.8	2.1	8.7	39	148	4.8	0.3	15
13	<0.1	1.1	–0.2	1.8	0.2	0.2	0.6	8.1	30	169	1.5	<0.1	73
4				no direction			0.3	6.9					
0.6				no direction			0.3	4.3					
MK2:													
503	0.6	2.5	–0.1	8.7	1.5	0.6	2.4	11.0	26	102	5.6	0.2	30
202	–0.8	2.9	<0.1	4.5	1.0	0.8	1.7	8.1	47	285	3.7	0.3	11
50	–1.0	3.7	–0.1	6.0	1.1	1.0	2.2	9.2	46	265	4.9	0.5	9
13	–0.4	2.4	–0.7	2.8	0.3	0.8	1.2	8.7	67	328	2.6	0.3	8
4				no direction			0.9	7.2					

mab = metres above bottom, *mag* = mean velocity magnitude, *V* = vector mean, *SF* = stability factor

b) Short-term moorings MK1 and MK2

The time covered by MK1 and MK2 proved to be a phase of very slow deep currents. Rotor stalls range between 46 and 89%, i. e. velocities were smaller than 1–1.5 cm/s which is the threshold velocity of the rotor (see Table 1). A comparably high percentage of rotor stalls was also observed by KONTAR AND SOKOV [1994] in the Clarion-Clipperton province of the northeastern tropical Pacific. Their current measurements (55 days, sampling interval 15 minutes) give comparable mean values and rotor stalls of 50% at 15 mab, and of 80% at 5 mab.

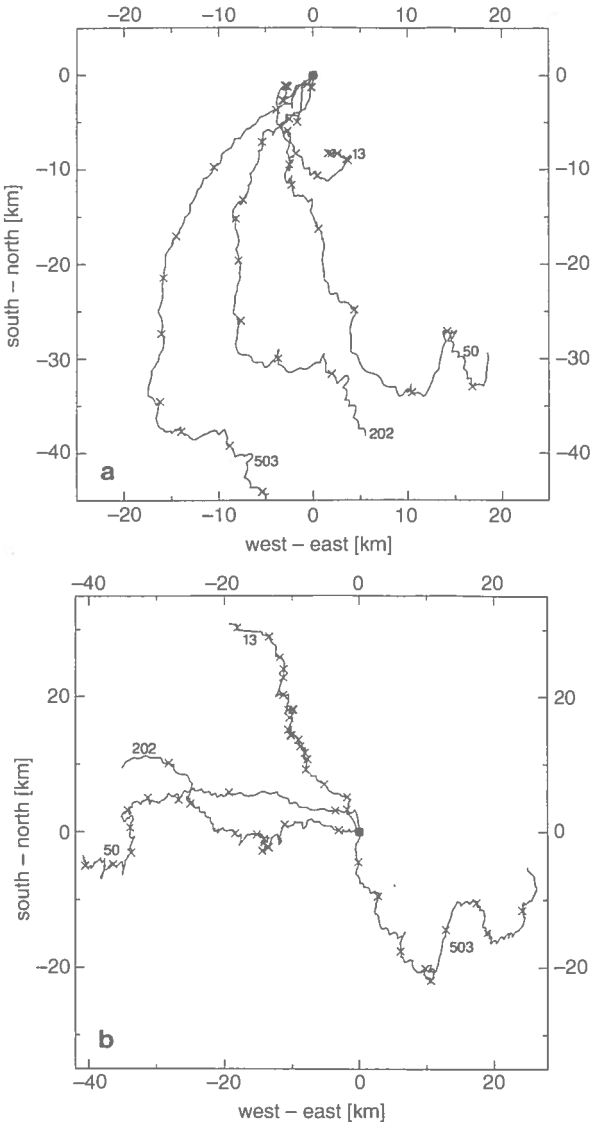

Fig.5: Progressive vector diagram of moorings MK1 (a) and MK2 (b). Time marks (x) are given every 5 days, the numbers at the tracks give the distance from bottom in metres.

At MK1, the mean velocity magnitudes are between 0.3 and 2.1 cm/s, with maximum velocities ranging from 4.3 cm/s at 0.6 mab to 6.7 cm/s at 50 and 503 mab. The PVD shows a mainly southward flow (Fig.5a). Time marks (x) are given every 5 days. The spacing of the time marks indicates a relatively regular flow between 50 and 500 mab. At 13 mab, the flow is extremely weak and there is a pronounced directional shear during the last 2 weeks of the record.

At MK2, mean magnitudes range from 0.9 to 2.4 cm/s, with maxima of 7.2 cm/s at 4 mab, and 11 cm/s at 503 mab. The PVD reveals a strong directional shear between 13 and 50 mab and between 200 and 500 mab (Fig. 5b). The spacing of the time marks is less regular than for MK1 and indicates the intermittent character of flow at this position.

Time series of all current meters (D1, MK1, MK2) are presented by KLEIN [1996].

The BBL and its sublayers

The term 'bottom or benthic boundary layer' is not standardized. Sometimes it is used as a synonym for bottom mixed layer, e. g. ARMI AND MILLARD [1976], or it is used in the biological sense as '... the sediment community and assemblage of organisms in the overlaying water column associated with the bottom (within 100 m of the seabed)' (SMITH AND HINGA [1983]). Here, the term BBL is used for that part of the water column which is in any way affected by the the seabed. Theoretically, the BBL can be subdivided into several sublayers which are distinguished by their hydrographical characteristics and/or their dynamical structure. Not all sublayers can be resolved by these measurements, and not all layers are necessarily fully developed or even existent. Nevertheless, if there is information about bottom roughness and near-bottom currents, the properties of the sublayers described below can be estimated by theoretical approaches.

Two parameters are essential for such estimates: bottom roughness, i. e. the question whether there are hydrodynamically rough or smooth conditions, and friction velocity u_* which can be estimated by the relation

$$u^* = \frac{U_g}{30} \tag{1}$$

with U_g the geostrophic velocity above the BBL (ARMI AND MILLARD [1976]). The D1 moorings give typical values for U_g, about 3 cm/s for periods of slow motion and up to 10 cm/s for periods with strong currents (KLEIN [1993]).

Regarding bottom roughness, we distinguish between areas covered with fine sediments and areas with manganese nodule coverage. The difference between hydrodynamically rough and smooth conditions is given by the Reynolds number:

$$R_e = \frac{\varkappa_s u_*}{\nu} \tag{2}$$

where $\varkappa_s$ is the roughness element or grain diameter, and ν the kinematic molecular viscosity for water (= 1 x 10^{-6} m^2s^{-1}). Under smooth conditions, R_e is smaller than 3, in rough conditions R_e is >70. The critical factor is the grain size, i. e. the nodule diameter. Even during periods of relatively strong currents >10 cm/s R_e is smaller than 3 (hydrodynamically smooth conditions) if the area is covered only with sediment. Rough conditions occur only if the bottom is covered with manganese nodules.

The deepest layer close to a smooth sea bottom is the very thin **viscous sublayer** (VSL). Its thickness Z_{vs} is only about 1–2 cm at U_g = 3 cm/s (WIMBUSH [1976]) but this is nevertheless significant for animals living close to the seabed (GAGE AND TYLER [1991]). Z_{vs} will decrease at an increase of U_g. If any structure, e. g. a manganese nodule or marine organism, exeeds one third of Z_{vs} the viscous flow is disrupted and becomes turbulent.

The **logarithmic layer** (*LL*) lies above the VSL. The velocity at height z, $U(z)$, is given by

$$U(z) = \frac{u_*}{\varkappa} \ln \frac{z}{Z_0} \tag{3}$$

where $\varkappa$ is the von Karmans constant (= 0.4) and Z_0 the roughness element (BOWDEN [1978]). Under hydrodynamically rough conditions Z_0 amounts to $\varkappa_s/30$, in the hydrodynamically smooth case Z_0 is $9\nu/u_*$. The height of *LL* is about 1 m. Within *LL*, the Coriolis force is negligible compared to viscosity and the stress is assumed to be constant.

The height of the turbulent **Ekman Layer** (*EL*) can be approximated by

$$h_e = 0.4 \frac{u_*}{f} \tag{4}$$

with Coriolis parameter f = 1.65 x 10^{-5} 1/s at the SEDIPERU site, and f = 1.77 x 10^{-5} 1/s at the DEA (BOWDEN [1978]). Ekman's theory predicts a decrease of velocity from the top of *EL* towards the bottom and veering of the current direction by 45° to the right (at southern latitudes) compared to the geostrophic flow above *EL*. This veering cannot be observed in our data because there is no information about the current direction below 13 mab (see Table 2). h_e versus U_g is shown in Fig. 7. Another relation for h_e is by the Ekman theory:

$$h_e = \pi \sqrt{\frac{2A_z}{|f|}} \tag{5}$$

where A_z is the vertical eddy diffusivity. Using [4] and [5] it is possible to estimate the order of magnitude of A_z inside the *EL*. For U_g = 1 cm/s A_Z is of the order of 1 cm^2/s, for U_g = 10 cm/s A_Z amounts to about 50 cm^2/s.

Including both *LL* and *EL*, the **bottom mixed layer** (BML) is defined by its hydrographical fine structure. Therefore, CTD probes and/or water samples are necessary to trace the height of this layer. Inside the BML, potential temperature, salinity, and other physical parameters are well mixed due to bottom friction.

CTD profiles from DEA obtained in 1992 give BML heights between 100 and 200 m (KLEIN [1993]). In 1996, during R/V 'Sonne' cruise 106/2,

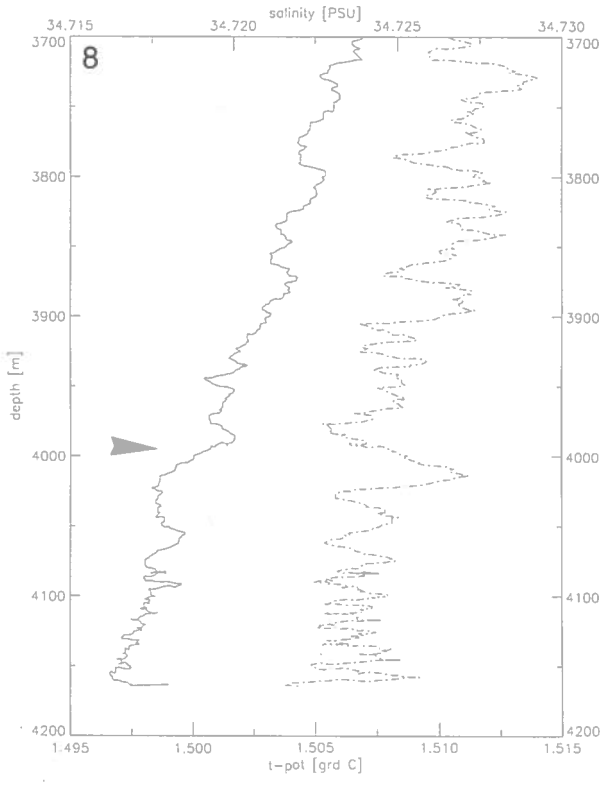

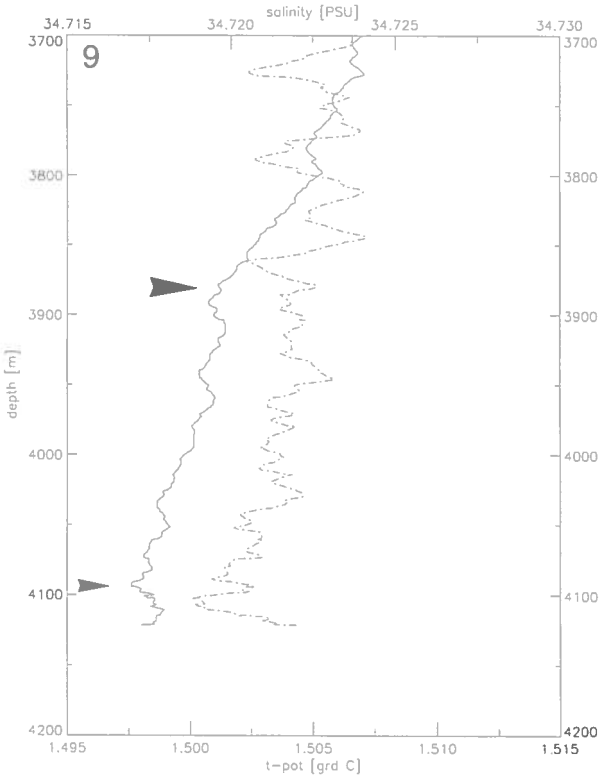

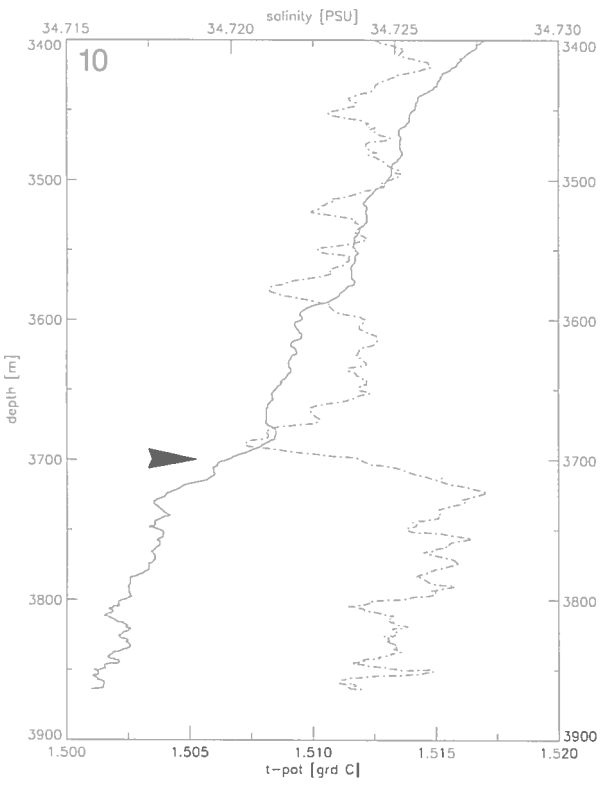

Fig.6: Near-bottom CTD profiles of stations 8, 9, and 10 showing potential temperature (solid line) and salinity (broken line). The arrows mark the top of an eroded bottom mixed layer. The small arrow at station 9 marks the top of the present BML. The position of the stations is shown in Fig.2.

three profiles were taken at the SEDIPERU site with a KMS 6000 multisonde manufactured by ME Meerestechnik Elektronic (Fig. 6). One profile was taken on top of a 250 m hill, another one at the foot of the hill running 1.5 nm to the east, and a third profile another 1.5 nm to the east in the abyssal plain very close to the MK1 position (see Fig. 2). Profiles 9 and 10 stopped at about 2–3 mab, profile 8 at about 10 mab because an additional chemical sampling system hung suspended from the CTD. All profiles were taken within 12 hours in a period of extremely low velocities. Nevertheless, there is a weak BML of at least 150 m height at all positions. The top of the BML is indicated by an arrow in Figure 6. It is the point where the slope of the curve changes due to bottom mixing. If the BML were homogeneously

mixed, the lower part of the curve would be a vertical line. However, because potential temperature and salinity are not homogeneously mixed the vertical gradients are significantly reduced. Possibly, we observe an eroded BML which was established during a period of higher velocity. At station 9 a small arrow indicates a second change of the potential temperature gradient which possibly marks the top of the present BML.

Light transmission data from the CTD probe give no hint of the existence of a bottom nepheloid layer. The height of this layer of enhanced turbidity frequently exceeds that of the BML significantly (NYFFELER AND GODET [1986]). Therefore, the height of the BML may be regarded as the upper limit of the BBL according to the above definition.

Discussion

The current data confirm earlier observations of WARREN [1981] and LONSDALE [1976]: The Peru Basin is an area of very weak bottom currents, and sometimes the flow is not 'current-like'. The mean currents are comparable to those in the Clarion-Clipperton province in the northeast Pacific (KONTAR AND SOKOV [1994]) but high-energy events like benthic storms have not been observed in the Peru Basin. Benthic storms are geographically related to sea-surface height variability, and the Peru Basin is an area of extremely low sea-surface height variability (0–4 cm, HOLLISTER AND NOWELL [1991]).

There are two types of erosional, nodule-free areas. Some of them are down-slope orientated, where the nodules are removed or buried by down-slope sediment slides. Other patches are orientated parallel to the slope (about 0.1 x 1 km), which might point to bottom currents (WIEDECKE AND WEBER [1996]). However, the observed bottom currents are not capable of causing erosion. Considering the extremely slow growth of nodules on the order of several hundred thousands of years, the cause may have been highly energetic bottom currents in earlier periods of the basin history.

The currents at MK1 and MK2 are not correlated. The distance between MK1 and MK2 is 117 nm, i. e. even with a mean speed of 5 cm/s a signal has a transit time of about 50 days from one mooring to the other. However, according to Robinson and KUPFERMAN [1985], current measurements in the deep central Pacific which are only 10 km apart may be distinctly different. This is confirmed by the small Lagrangian length and time scales (TAYLOR [1921]) ranging between 0.4 and 5.6 km (respectively 0.5 to 6.0 days) for MK1 and MK2 (see Table 3). The values are calculated from low-passed data, i. e. tidal and inertial motions are removed. If periods of higher kinetic energy occur in the records, as at long-term mooring D1, the values increase by about one order of magnitude. This holds also true for the eddy diffusivities $k_{x,y}$. Due to the large number of rotor stalls at MK1 and MK2, the values cannot be calculated for the deeper current meters. This strong local variability makes it difficult to assess the impact of mining operations, because

Table 3

Lagrangian statistics, low-passed data (48 hours)

mab	T_x	T_y	L_x	L_y	k_x	k_y
m	days		km		$cm^2/s \times 10^5$	
D1:						
200	9.3	11.5	14.7	17.3	27.07	30.20
50	6.7	14.8	11.1	27.2	21.44	57.98
30	5.7	13.8	10.4	26.2	22.10	57.25
15	5.8	15.4	12.4	40.7	26.34	71.80
MK1:						
503	6.0	0.7	5.6	0.5	5.99	0.43
202	4.3	0.6	3.6	0.5	3-58	0.40
50	0.8	1.6	0.6	1.9	0.55	2.61
MK2:						
503	0.7	2.5	0.5	3.2	0.34	4.86
202	2.0	1.7	1.7	1.3	1.68	1.12
50	3.6	0.5	4.0	0.4	5.16	0.40

mab = metres above bottom, *x* = zonal, *y* = meridional
$T_{x,y}$ = Lagrangian integral time scale
$L_{x,y}$ = Lagrangian length scale, $k_{x,y}$ = eddy diffusivity

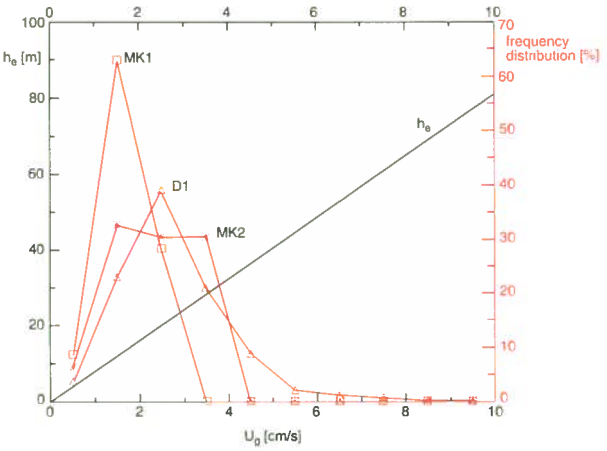

Fig.7: Thickness of the Ekman layer h_e estimated according to [4] and percentage frequency distribution of U_g (1 cm/s intervals) as observed at MK1 and MK2 at 504 mab (52 days), and at D1 at 200 mab (861 days). U_g is averaged over the respective 4 preceding days which is the time scale for the maintenance of the Ekman layer.

extrapolations from a few measurement positions may be unreliable for a larger area.

Because of the manganese nodule coverage, there will be no viscous sublayer, i. e. the flow will be turbulent directly above the sea bed. The logarithmic layer is of the order of 1 metre. The height of the Ekman layer varies according to [4]. The time scale of the EL is of the order of half a pendulum day (Bowden [1978]), i. e. 106 hours at the SEDIPERU site and 98 hours at the DEA site. Therefore, not any increase in the current speed will cause an expansion of the *EL*, but the speed level must be maintained for about 4 to 5 days.

Figure 7 shows the percentage frequency distribution of the mean (geostrophic) flow U_g for MK1 and MK2 at 503 mab – which is clearly outside the BBL – and for D1 at 200 mab. The mean velocity magnitude used for this diagram is a mean over the respective 4 preceding days, i. e. the velocity which is available for maintaining the Ekman layer. During periods of slow bottom currents (MK1, MK2) we can expect an Ekman layer height of between 10 and 30 m. The D1 time series which covers a much broader time interval (861 days) with several events of relatively strong currents shows that h_e can reach values up to 60 m during such events. Figure 8 presents a time series of U_g (4 day average) and h_e at D1. On average h_e amounts to 20 m, but there are also periods of 1 to 2-month duration with values of about 40 m and even higher values.

Armi and Millard [1976] found a correlation between BML height and the daily mean value of the 'outer' flow. The recordings at MK1 between 50 and 503 mab ended a few days before the CTD profiles shown in Figure 6 were taken, but the daily mean value at 0.6, 6, and 13 mab gives a current speed of less than 1 cm/s. Therefore, the weak BML's we observe in the profiles can be regarded as a relict of an old BML which has been established during an earlier period of stronger flow.

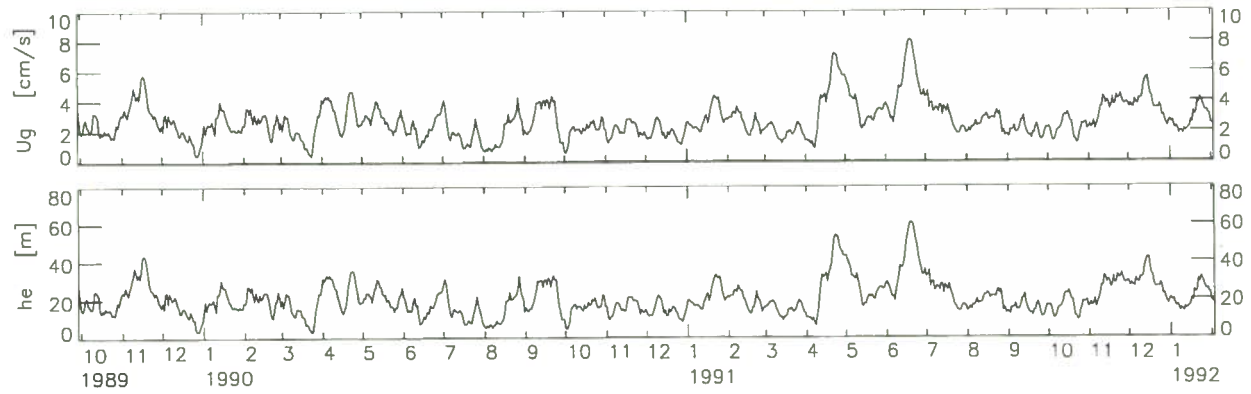

Fig.8: Daily mean values of Ekman layer height h_e (top) und mean geostrophic velocity U_g at D1 200 mab (bottom). U_g is averaged over the respective 4 preceding days which is the time scale for the maintenance of the Ekman layer.

Portions of a well-mixed layer can also be advected away. The daily means at 202 and 503 mab range between 0 and 4 cm/s with a great day-to-day variability. The BML height varies according to the mean values and stabilizes only during periods of stronger flow which last 4–5 days at MK1, or several weeks at D1. Numerical estimates of BML height h_0, for example those given by RICHARDS [1990] for modelling purposes, provide too small values compared to the observations presented above (of the order of h_e). But h_0 is also directly related to U_g and will therefore vary in the same way as h_e (see Fig. 8). ARMI AND MILLARD [1976] estimated h_0 to be approximately 6 times the Ekman layer height, which agrees fairly well with the above observations.

Observations of the temporal variability of BMLs are well documented from different Atlantic sites, e. g. by ARMI AND MILLARD [1976] and KLEIN [1987]. Pulsations of the deep flow like those observed at D1 are also known from the deep NE-Atlantic (KLEIN AND MITTELSTAEDT [1992]), where periods of stronger near-bottom flows observed in the bottom 1500 m have a duration of 1 to 2 month. Definite causes of the forcing and vertical extension of pulsations in the Peru Basin have not been found, however. Driving mechanisms like deep-reaching mesoscale eddies have not been observed in the data. Possible mechanisms are episodic spill-overs similar to those described by LONSDALE [1980] for deep water exchange in the Panama Basin by spill-overs from the Peru Basin.

Conclusions

Beside the 'long-term' alternation between periods of weak (1–3 cm/s) and strong (>5 cm/s) near-bottom flow with typical time scales of 3 to 5 months, there is a strong day-to-day variability of daily mean values during periods of weak currents. Therefore, stable BBL's can only be expected during periods of strong currents. The variation of the daily mean flow often is faster than the time necessary to build up a BML. During times of mean values <1 cm/s, the BBL and its sublayers might break down completely, i. e. the BML is no longer maintained but eroded. The tidal currents are too weak to produce enough turbulent energy for the permanent maintenance of a strong BML. The transition between hydrodynamically smooth and rough condition is controlled primarily by the grain size, respectively nodule diameter.

The local and temporal variability makes it difficult to properly assess the impact of mining operations and to model the physical environment, especially for a larger area. The extent of a disturbance will depend strongly on the – unpredictable – hydrodynamical situation on the sea bed. This holds particularly for biological systems which react very sensitively to extreme values. To obtain better estimates which not only give orders of magnitude, a quasi-synoptic pattern of CTD stations and a mooring grid of less than 10 km is required.

Acknowledgements

The Bundesministerium für Forschung and Technologie supported DISCOL under grants 03R389, 392, 396, 411, 417, and 03F0010F. The Bundesministerium für Bildung, Forschung und Technologie funded ATESEPP under contract numbers 03-G-0106 A-I.

References

ARMI, L. AND R. C. MILLARD, 1976: The bottom boundary layer in the deep ocean. *J. Geophys. Res.*, **81**, 4983–4990.

BERNER, R. A., 1976: The benthic boundary layer from a viewpoint of a geochemist. In: 'The benthic bottom boundary layer', Ed.: I. N. McCave, pp. 33–56, New York: Plenum Press.

BOWDEN, K. F., 1978: Physical problems of the benthic boundary layer. *Geophys. Surv.*, **3**, 255–296.

GAGE, J. D. AND P. A. TYLER, 1991: Deep-Sea Biology: A natural history of organismns at the deep-sea floor. Cambridge: Cambridge Univerity Press, 504 pp.

HOLLISTER, C. D. AND A. R. M. NOWELL, 1991: HEBBLE epilogue. *Marine Geology*, **99**, 445–460.

Jankowski, J. A. und W. Zielke, 1995: Mesoskalige Stofftransporte im Pazifik als Folge des Tiefseebergbaus. Institut für Strömungsmechanik und Elektronisches Rechnen im Bauwesen der Universität Hannover, 84 pp.

Klein, H., 1987: Benthic storms, vortices, and particle dispersion in the deep West European Basin. *Dt. Hydrogr. Z.*, **40**, 87–102.

Klein, H. and E. Mittelstaedt, 1992: Currents and dispersion in the abyssal Northeast Atlantic. Results from the NOAMP field program. *Deep-Sea Res.*, **39**, 1727–1745.

Klein, H., 1993: Near-bottom currents in the deep Peru Basin, DISCOL Experimental Area. *Dt. Hydrogr. Z.*, **45**, 31–42.

Klein, H., 1996: Current measurements in the deep Peru Basin, Data Report. Technical Report Forschungsverbund Tiefsee-Umweltschutz, c/o Bundesamt für Seeschiffahrt und Hydrographie, 72 pp.

Kontar, E. A. and A. V. Sokov, 1994: A benthic storm in the northeastern tropical Pacific over the fields of manganese nodules. *Deep-Sea Res.*, **41**, 1069–1089.

Lonsdale, P., 1976: Abyssal circulation of the Southeastern Pacific and some geological implications. *J. Geophys. Res.*, **81**, 1163–1176.

Lonsdale, P., 1980: Manganese-nodule bedforms and thermohaline density flows in a deep-sea valley on the Carnegie Ridge, Panama Basin. *J. of Sedimentary Petrology,* **50**, 1033–1048.

Nyffeler, F. and Ch.-H. Godet, 1986: The structural parameters of the benthic nepheloid layer in the northeast Atlantic. *Deep-Sea Res.*, **33**, 195–207.

Richards, K. J., 1990: Physical processes in the benthic boundary layer. Philosophical Transactions of the Royal Society of London, Series A, 331, 3–13.

Robinson, A. R. and S. L. Kupferman, 1985: Dispersal from deep ocean sources: Physical and related scientific processes. Sandia National Laboratories, Albuquerque,Report SAND82-1886.

Schriever, G., 1995: DISCOL – Disturbance and recolonization experiment of a manganese nodule area of the Southeastern Pacific. Proceedings of the ISOPE – Ocean Mining Symposium, Tsukuba, Japan, November 21–22, 1995.

Schriever, G., A. Koschinsky und H. Bluhm, 1996: Cruise Report ATESEPP. Berichte aus dem Zentrum für Meeres- und Klimaforschung, Reihe E, Nr. 11, 195 pp.

Smith, K. L. and K. R. Hinga, 1983: Sediment community respiration in the deep-sea. In: 'The Sea', Vol. 8, Ed.: G. T. Rowe. Wiley Interscience, New York, 331–370.

Taylor, G. I., 1921: Diffusion by continuous movements. Proc. London Math. Soc., A20, 196–211.

Thiel, H. and G. Schriever (Eds.), 1989: Cruise report DISCOL 1, SONNE-cruise 61. Institut für Hydrobiologie und Fischereiwissenschaft der Universität Hamburg, 75 pp.

Thiel, H., G. Schriever, H. Bluhm, Chr. Bussau und Chr. Borowski, 1994: Abschlußbericht für die Bewilligung 03F 0010 F im BMFT-Projekt „Wiederbesiedlung nach der mechanischen Beeinflussung eines Manganknollenfeldes in der Tiefsee des Süd-Pazifiks – DISCOL". Berichte aus dem Zentrum für Meeres und Klimaforschung, Reihe E, Nr. 8, 60 pp.

Thiel, H. and Forschungsverbund Tiefsee-Umweltschutz, 1995: The German environmental impact research for manganese nodule mining in the SE Pacific Ocean. Proceedings of the ISOPE – Ocean Mining Symposium, Tsukuba, Japan, November 21–22, 1995.

von Stackelberg, U., 1997: Growth history of manganese nodules and crusts of the Peru Basin. In: Nicholsen, K., J. R. Hein, B. Bühn and S. Dasgupta (Eds.): Manganese mineralisation: Geochemistry and mineralogy of terrestrial and marine deposits. Geological Society Special Publication No.19, 153–176.

Warren, B. A., 1981: Deep circulation of the world ocean. In: B.A. Warren and C. Wunsch (Eds.): Evolution of physical oceanography. Cambridge: MIT Press, 6–41.

Wiedecke, M. H. and M. E. Weber, 1996: Small-scale variability of seafloor features in the northern Peru Basin: Results from acoustic survey methods. *Marine Geophys. Res.*, **18**, 507–526.

Wimbush, M., 1976: The physics of the benthic boundary layer. In: 'The benthic boundary layer', Ed.: I. N. McCave, pp. 3–10, New York: Plenum Press.

Submitted: 20. 5. 1997
Accepted: 10. 7. 1997

Address of author:

Holger Klein
Bundesamt für Seeschiffahrt und Hydrographie
20539 Hamburg
Bernhard-Nocht-Straße 78
email: holger.klein@bsh.d400.de